Chalcogenide Letters Vol. 19, No. 9, September 2022, p. 651 - 662

Study on preparation and characterisation of pure and lithium incorporated SnS thin films for solar cell applications

C. N. Omprakash Anand[a,*], P. Thirunavukkarasu[a], A. Balamurugan[b*], S. Surendhiran[c]
[a]*Department of Electronics, Sri Ramakrishna Mission Vidyalaya College of Arts and Science, Coimbatore – 641 020, Tamilnadu, India*
[b]*Department of Physics, Government Arts and Science College Avinashi – 641654, Tamilnadu, India*
[c]*Centre for Nanoscience and Technology, KS Rangasamy College of Technology Tiruchengode – 637 215, Tamilnadu, India*

A ternary transition metal sulfide was synthesized and characterized by the sonochemical approach in this study, namely a Li (Li) and tin sulfide (SnS) thin film incorporating lithium (Li). Lithium incorporated SnS thin films (Li-SnS) were synthesized by equal molar ratios used in the synthesis approach. In these prepared thin films, the crystallite size averaged 5 nm and the thin films were of good crystalline nature. Nanoparticles in the thin film samples have a uniform sphere shape, with clusters forming in a few places, as seen by FE-SEM images. The presence of Li, Sn and S was confirmed through XRF spectral analysis. From the fingerprint region of the FTIR spectra, the presence of Ni, Li, Sn and sulphur was confirmed and no other impurities were detected. The UV absorption analysis was highly indicating the enhanced photon absorption behaviour of the prepared thin film samples due to the incorporation of Li with SnS samples. The efficiencies of the solar cell fabricated with SnS, Li-SnS, were found to be 6.21 and 7.92 %. From the results it is concluded that Li-SnS thin film samples can be a potential candidate for use as an electrode in solar cell applications.

(Received April 7, 2022; Accepted September 28, 2022)

Keywords: Tin sulphide thin films, Lithium incorporation, Sonochemical technique, Solar cell applications

1. Introduction

Ternary metal sulphide compounds have received a lot of attention because they offer promising opportunities to meet the challenges of the environment, energy, as well as sustainability. The synthesis of high-performance thin film materials with easy recollection and high stability with low toxicity remains critical in the development of highly efficient energy conversion systems. Because of their potential applications in energy conversion and environmental cleaning, inorganic metal sulphide compounds have grown in popularity. Among the various metal sulphides researched in recent years is tin sulphide (SnS), an n-type semiconductor with adjustable band gap behaviour and minimal processing effects.

In particular, thin films of pure tin sulphide (SnS) may be used in solar cells, batteries, supercapacitor, and nanoparticles for energy storage and conversion processes. SnS is a semiconductor compound with p-type conduction that belongs to the group IV–VI chalcogenides. Photovoltaic devices have received an increasing amount of attention. Based on the cationic and anionic vacancies present, it has either a direct or indirect band gap. Solar cells can benefit from SnS as an absorber material because it possesses ideal electronic properties, including an optimal optical bandgap, high optical absorption coefficient, and intrinsic p-type conductivity. SnS-based solar cells, however, tend to have power conversion efficiencies (η) far below 4%, with few exceptions. To improve the efficiencies of the SnS thin films based solar cell, there must be a

* Corresponding author: bala.snr@gmail.com
https://doi.org/10.15251/CL.2022.199.651

modification or alteration need. Especially, ternary metals or metal oxides or metal sulfides as a dopant may be the best choice for this problem.

Transition metals like Lithium (Li) materials demonstrated their superiority in energy storage and conversion applications such as dye-sensitized solar cells, sodium-ion batteries, lithium-ion batteries, as well as supercapacitors. Due to the existence of nickel and cobalt ions in compared to other metal sulphides, they are also expected to provide massive support for SnS thin films for solar cell applications. Unique morphologies as well as compositions can improve the electrochemical performance of Li, which could be prepared utilising sol gel, hydrothermal, solvothermal, template method, electrodeposition, microwave-assisted methods, and so on. Among all these synthesis methods, the sonochemical method offers significant advantages for the synthesis of nanomaterial. The sonochemical technique has been shown to be an environmentally friendly technique for creating highly stable nanomaterial with uniform morphology and less particle size. Sonochemical approaches have resulted in a non-toxic, short reaction time, ultrafine high yield production. As a result of the massive benefits of sonochemical techniques, numerous unique nanomaterial are produced in the irradiated solution.

We demonstrated the SnS and Li incorporated SnS thin films as an electrode for solar cell applications in this article. The thin films mentioned above have been successfully synthesised using a sonochemical method and then coated using spin coating techniques. The preparing thin films by spin coating technique have several advantages, including faster deliveries at a low cost, a shorter deposition time, being environmentally friendly, and producing uniform films with good adhesion. UV-Vis spectroscopy (UV) and photoluminescence (PL) analysis were used to characterise the optical properties of the prepared thin films. A range of imaging techniques, including scanning electron microscopy (SEM), scanning probe microscopy (SPM), transmission electron microscopy (TEM), and particle size analysis (PSA) have been used to identify the morphology and particle size. Infrared spectroscopy was used to inspect the chemical compositions of the thin films, and IV measurements were taken to demonstrate their potential for solar cell applications.

2. Experimental

2.1. Materials

Lithium (II) chloride, stannous chloride, Sodium Sulphide flakes, Ammonia, Indium tin oxide slides (ITO, surface resistivity 70-100 Ω/sq.) and N-Methylpyrrolidine (NMP) were purchased from Sigma Aldrich. Distilled water was utilized as solvent. All the AR grade chemicals were utilized without further purification.

2.2. Method

A probe type Sonicator was employed in the sonochemical technique used to synthesis the SnS, Ni-SnS, Co-SnS, NC-SnS nanoparticles. A 100 mL of stannous chloride solution (0.1 M) was taken in a beaker and placed in sonication chamber. Initially, the ultrasonic waves was irradiated for 30 mins then the 1M of ammonia solution was added drop wise into it till the pH reaches nearly 10; again the solution was placed in sonicator for 210 mins with 40 kHz power of irradiation.

To carry out the purification process, the mixture was sonicated followed by centrifugal separation and supernatant removal; the sediment was then dispersed in fresh ethanol (20 ml) in the sonicator for 15 minutes; the suspension obtained was centrifuged, the supernatant was detached, and the sediment was re-suspended in fresh ethanol (20 ml) in the sonicator for 15 minutes (this was repeated twice). In the end, we obtain an ethanol suspension. Using a hot air oven at 80 degrees Celsius, the obtained solution was dried to obtain ultrafine nanoparticles. Using mortars and pistols, finely ground powder was obtained. The resulting powder was called SnS nanoparticles.

For the synthesis of Li incorporated SnS nanoparticles; 0.1 M of lithium chloride solutions was added separately to the SnS solution in aforementioned procedure. The final product of this procedure was named as Li-SnS nanoparticles.

In 50 mL N-Methylpyrrolidine (NMP) was mixed with the prepared SnS and Li-SnS nanoparticles. During 80 °C stirring, the solution was changed into a crystalline form of 20 mL. In the hot-air oven, the ITO plates were then cleaned with acetone, rinsed with deionized water, and finally dried. We then cut the ITO plates into 1 cm^2 pieces. SM 108 BT; Sawatec, Ruggell, Switzerland) was loaded into the spin-disk coater. ITO substrates were coated with 1 mL of the coating solution at 3000 rpm for 30 seconds. After deposition, the film was dried in an oven at 150 °C for 10 minutes to remove unwanted residuals and achieve well-crystallized films. The temperature was kept at 25 °C during the spin-coating process. The coating and drying process was repeated three times until the desired thickness was reached. To produce highly crystalline thin films, the thin films were heated in the air for 15 minutes at 400°C.

2.3. Sample preparation for electrochemical and IV measurements

A Keithley 2400 source metre and a Newport solar simulator (model no.91160) with AM 1.5 G spectrum supply were used to measure the IV. The anode material in the DSSC cell was SnS and LiSnSnano powders. Furthermore, all of the Nano powder was weighed individually, followed by the addition of Acetyl Acetone with two drops of Criton X-100, and the mixture was continually combined with a mortar until slurry formed. On the conductive side of the ITO glass, a 1 cm^2 window were cut out of Scotch Magic tape and placed. Distinct slurrys of SnS and LiSnS nanoparticles were put to the ITO glass. The heating takes 30 minutes at 450°C. After immersing the samples inside the Ruthenium N71 dye for 12 hours, the cell was constructed with a platinum-coated electrode as well as a lithium iodide liquid as the electrolyte.

2.4. Physical and electrochemical characterization

The phase purity of SnS and Li-SnS thin films were confirmed by X-ray diffraction studies (XRD; X'Pert PRO, PANalytical, Almelo, the Netherlands). The surface morphology of SnS and Li-SnS thin films were analyzed by FE-SEM (JSM, JEOL 7600F). The presence of Sn, Li, and S were observed by energy dispersive X-ray analysis (XRF). The functional groups and chemical composition of the SnS, and Li-SnS, thin films were analyzed using a FTIR spectrophotometer (Spectrum 100; USA) in the range 4000-400 cm^{-1}. The average particle size distributions of SnS and Li-SnS nanoparticles are investigated with Nanophox particle size analyzer (Sympatec Germany). UV-vis absorption spectra of SnS and Li-SnS thin films were recorded using Agilent Cary 8454 (Singapore) spectrometer. The electrochemical analyses such as impedance spectroscopy (EIS), linear sweep voltammetry (LSV), was analysed by Autolab (PGSTAT302N MetrohmAutolab, the Netherlands) in 6M KOH at room temperature. SnS and Li-SnS thin films, platinum wire, and saturated calomel were utilized as the working electrode, counter electrode, and reference electrode, respectively.

An in situ scanning probe microscopy (SPM) coupled with a Berkovichnanoindenter was used to assess the hardness (H) of the nanostructured coating utilising quasistatic software to characterise surface-related parameters such as topographical images, roughness, and hardness over all thin film samples. The predicted specimen (10 m^2 area) was subjected to a maximum load of 500 N for 15 seconds, with a loading and unloading force rate of 100 N/s and a 5-second holding time.

3. Results and Discussion

Figure 1 depicts X-ray diffraction (XRD) patterns of SnS and Li doped SnS thin films with equal molar concentrations of Li. According to XRD analysis, the fabricated films have a polycrystalline structure with an orthorhombic arrangement, and their orientations are oriented strongly along the directions (210) and (111) because their intensity is higher than other planes. The structural data of the prepared SnS: Li thin films were in perfect agreement with that in the standard JCPDS card number 39-0354. For the peaks at 2 = 26.0°, 31.5°, 39.0°, 45.5°, and 51.3°, the SnS thin films are indexed with (120), (111), (131), (002), and (151). The X-Ray diffraction results indicate that both layer orientation and crystal quality improves when Lithium ions are

added to SnS nanoparticles. However, no additional peaks appear when lithium ions are introduced.

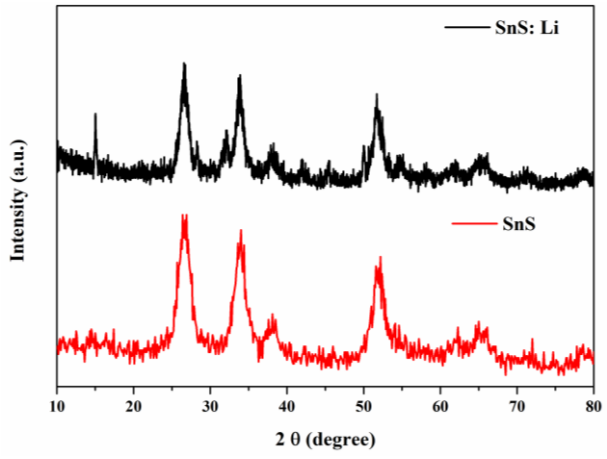

Fig. 1. XRD patterns of the prepared SnS and SnS: Li thin films.

In the study of SnS and SnS: Li thin films, Debye Scherer's relation were used to determine their crystal size (D). An average crystal size of 8.91 nm was calculated for SnS and a crystal size of 12.4 nm for SnS: Li. SnS nanostructures contain Li ions that cause the crystal surface area to increase due to the larger ionic radii of Li ions than those of Sn ions. Resulting crystal packing of pure SnS nanoparticles shrank due to these factors. This could explain the increase in crystal size of the prepared SnS: Li thin films when compared to undopedSnS thin films.

The FTIR spectra of SnS and SnS: Li thin films are presented in Figure 2. In both films, peaks at 400 and 800 cm^{-1} can be seen due to the characteristics of SnS. In SnS, characteristic vibrational peaks are observed between 2640 and 2680 cm^{-1} due to the presence of OH groups contained within the samples. However, in SnS: Li nanoparticles, the typical peaks are observed at 454 and 560 cm^{-1}, respectively. The FTIR profiles of all samples coincided with the XRD results, indicating that Sn, S, and Li ions are present in the sample. The SnS: Li sample exhibits two distinct peaks at 613 cm^{-1} and 658 cm^{-1}, respectively for Sn-S and Li-S complex group stretching vibrations.

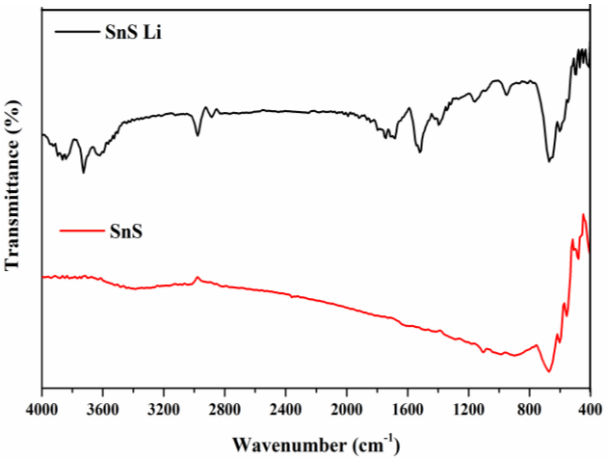

Fig. 2. FTIR Spectra of the prepared SnS and SnS: Li thin films.

Table 1 illustrates the quantitative elemental disseminations of SnS, and Li: SnS nanoparticles. The presence of tin, Lithium and sulphur in the synthesised material were confirmed. The results clearly depict the uniform distribution of Sn, Li and S as per the proposed ratio taken in synthesis process.

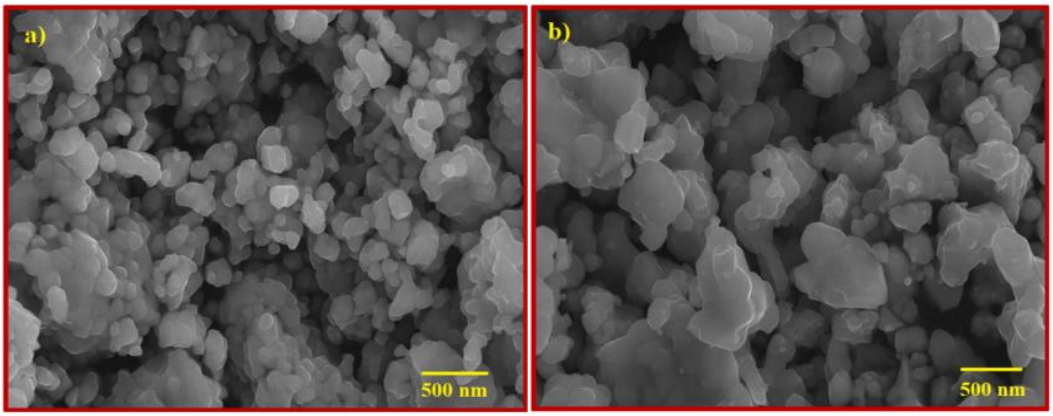

Fig. 3 FESEM images of the prepared SnS and SnS: Li thin films.

Figure 4 shows the particle size distribution analysis of the prepared SnS and SnS: Li nanoparticles. The majority of the nanoparticles were also smaller than 65 nm in size. However, a few coarser particles with sizes ranging from 80 to 100 nm are also observed, which can be attributed to the nanoparticles' agglomeration behaviour. The mean particle size of the rehearsed SnS and SnS: Li nanoparticles were measured to be 13.72 and 17.19 nm, respectively. When compared to undopedSnS, the average size of the SnS: Li is likely to improve. This is evident in the XRD analysis of the prepared SnS and SnS: Li nanomaterial and then also fully supports the XRD results.

Table 1. X-ray fluorescence spectral results of SnS, and Li: SnSnanoparticles

Analyst	**SnS**		**Li: SnS**	
	Weight %	**Atomic %**	**Weight %**	**Atomic %**
Sn	78.6	81.9	38.6	41.1
S	21.4	18.1	19.9	18.2
Li	0	0	41.5	40.7
Total	**100**	**100**	**100**	**100**

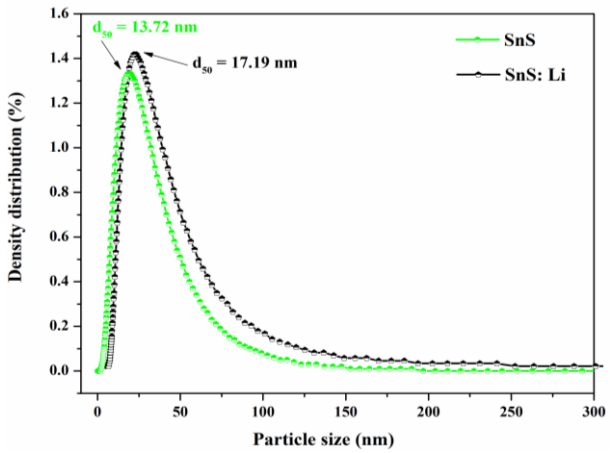

Fig. 4. Average particle size distribution of the prepared SnS and SnS: Li thin films.

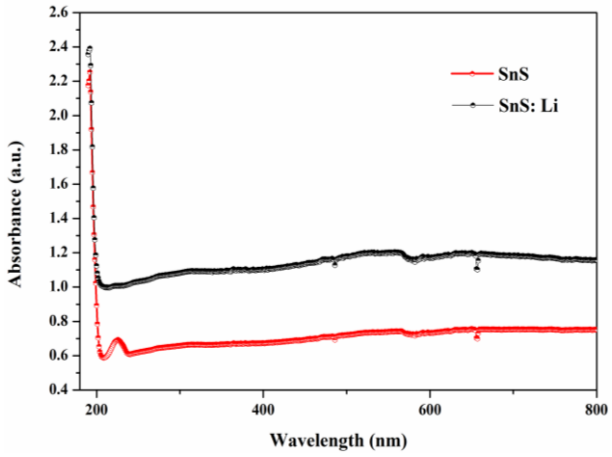

Fig. 5. UV-Vis spectra of the prepared SnS and SnS: Li thin films.

Figure 5 depicts the UV–Visible absorbance spectra of colloidal solutions of synthesised SnS and SnS: Li nanoparticles. Three absorbance peaks were observed in the absorbance spectra of ablation SnS nanoparticles. The first two peaks were found in the UV zone at 220 and 320 nm, respectively, whereas the third appeared as a band outside the UV region between 500 and 800 nm. The UV–Visible spectrum of SnS: Li exhibited three absorption peaks: one at 210 nm, one in the intermediate zone between the UV and visible areas at 485 nm, and one in the visible region as a wide band from 600 nm to 700 nm. As demonstrated in Figure 5, the absorbance level drops when Lithium ions are added to SnS nanoparticles.

The Tauc plot and optical direct band gap energy of thin films formed following the addition of Li ions to SnS nanoparticles are shown in Fig. 6. The optical direct band gap energy has been marginally enhanced, as can be shown. SnS and SnS: Li thin films with computed energy Band gaps of 3.09 and 3.14 eV, respectively. This obtained result clearly shows that the energy bandgap of the SnS nanoparticles can be tuned by doping the other metal ions with it.

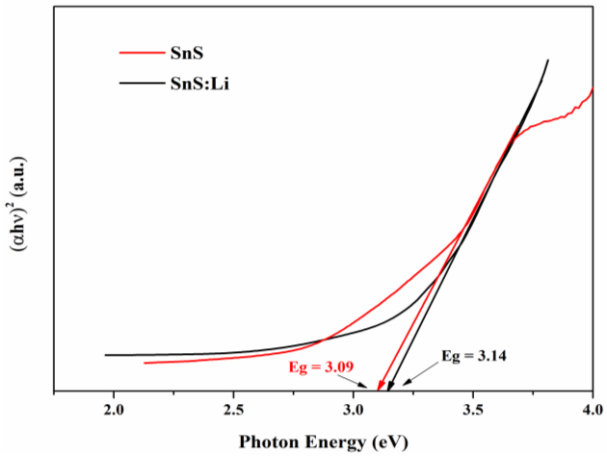

Fig. 6. Energy band gap images (Tauc plot) of SnS and SnS: Li thin films.

Surface roughness as well as hardness seems to be critical properties that can affect the electrochemical properties of nanomaterials. Figure 6 depicts the surface nano - indentation figures of SnS and SnS: Li thin films. An indentation of each five-point result on the load–displacement curve under experimental conditions revealed nearly identical reliability and validity of surface coatings. SnS as well as SnS: Li thin films have slightly higher elastic modulus, hardness, and roughness values. Figure 7 depicts topographical images of SnS as well as SnS: Li thin films in two-dimensional (2D) and three-dimensional (3D). During the electrochemical reactions, the SnS and SnS: Li thin films offered a strong protection to the surface of the ITO plates. In table 2 gives the hardness values, elastic modulus and roughness of the prepared samples.

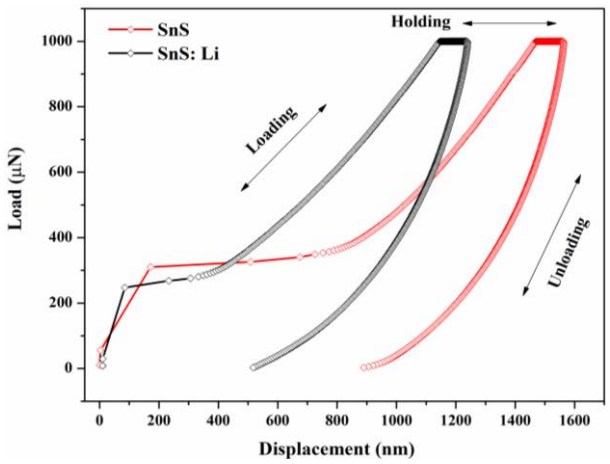

Fig. 7. Nano indentation test images of SnS and SnS: Li thin films.

A rehearsed SnS and SnS: Li thin film was also investigated using electrochemical impedance spectroscopy (EIS). Based on impedance spectra, we observe a major depression semicircle in the high-frequency region and a straight line in the low-frequency region for an ideal electrical double-layer capacitor (EDLC). Both SnS and SnS: Li thin films in the low-frequency region exhibit near-uniform vertical lines along their imaginary impedance axes, indicating perfect capacitive behavior.

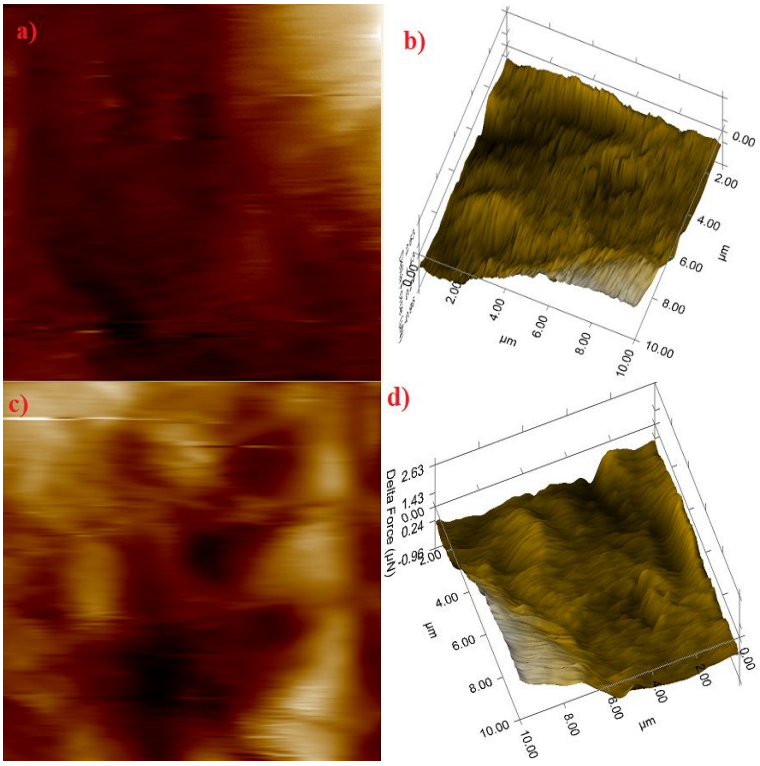

Fig. 8. Surface topographical images of SnS and SnS: Li thin films.

Table 2. Nano indentation studies surface parameters of SnS and SnS: Li thin films.

Substrate	Elastic modulus (MPa)	Hardness (MPs)	Average roughness Ra (nm)	Contact stiffness (µN/nm)
SnS	432.05	21.81	157.58	1.24
SnS: Li	754.48	59.04	65.598	1.84

Rs are equal to the sum of the ionic solution resistance, the inherent resistance of the active material, and the electrode/electrolyte resistance at the intersection with the real impedance axis and also the arc resistance. As well as that, the diameter of the arcs appears to be associated with Rct when measured in conjunction with double-layer capacitance. It appears that SnS: Li thin films promote more charge transfer since their arc radius is smaller.

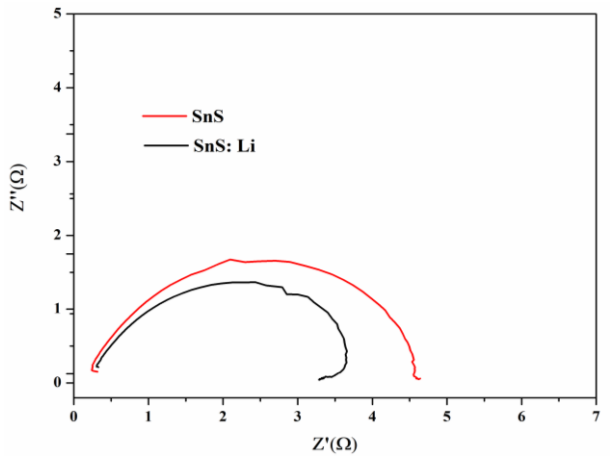

Fig. 9. Electrochemical impedance spectra of SnS and SnS: Li thin films.

Figure 9 depicts the potentiodynamic polarisation curves or Tafel plots of SnS and SnS: Li thin films in 6M KOH electrolytic solutions. Table 3 shows how the Tafel plot has been used to calculate electrochemical corrosion parameters such as corrosion rate (CR), corrosion potential (Ecorr), corrosion current (Icorr), and polarisation resistance (Rpol). A potentiodynamic polarisation experiment on SnS and SnS: Li thin films revealed that the ITO plates were anodically polarised. Both coated plate's exhibit greater corrosion protection than reported earlier. SnS: Li thin films have a higher corrosion potential (Ecorr) than SnS thin films. This clearly shows that the corrosion rate of SnS thin films (121.89 mm/year) is relatively low than those of SnS: Li thin films (216.67 mm/year). SnS and SnS: Li thin films displayed an increased polarisation resistance due to the oxygen reduction of Li ions. As a result of the presence of Li ions , Li thin films exhibit a more significant reduction of oxygen in 6M KOH electrolytic solution. SnS and SnS: Li thin films have been shown to exhibit improved electrochemical properties when compared to previous research (both EIS and LSV). The electrochemical analysis of SnS and SnS: Li thin films revealed they have better corrosion resistance and electrochemical performance.

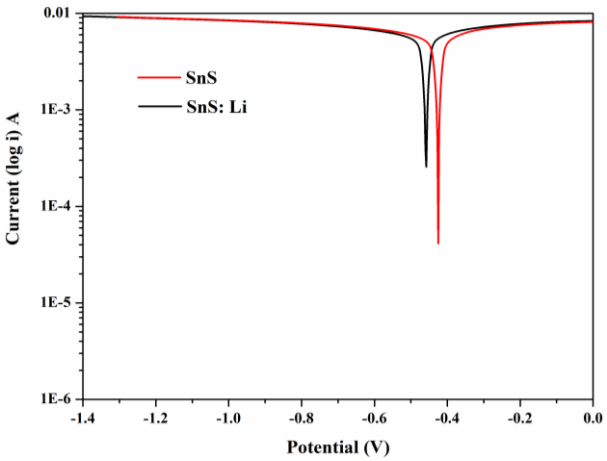

Fig. 10.Tafel plot of SnS and SnS: Li thin films.

Table 3. Tafel plot parameters of C: SnS, G: SnS and G: SnCdS thin films.

Substrate	Ecorr (mV)	Icorr (mA)	Polarisation resistance (Ω)	Corrosion rate (mm/yr.)	Improved efficiency (%)
SnS	-451.3	18.64	4.549	216.67	
SnS: Li	-456.1	10.49	6.326	121.89	43.74

4. Photovoltaic performances of the SnS and SnS: Li thin films

Current Voltage (J-V) (Figure 11) shows the properties of the prepared SnS and SnS: Li thin films. Forward bias is used for J-V Characterization. For SnS and SnS:Li doped films, the rated voltage that induces the current rise varies. Table 4 lists photovoltaic properties for SnS and SnS: Li thin films. The open circuit voltage for SnS is roughly 1.246 V, whereas for SnS: Li it is around 1.255 V. There is a limit to how much voltage can be accommodated in semiconductor materials, such that breakdown voltages can be obtained.

It's also worth noting that upon reaching the breakdown voltage, the current density in chemically and greenly synthesised samples, as well as Li ions doped samples, is higher. In the crystal of green synthesised SnS thin films, doping liberates more free electrons and holes. Conduction is aided by the presence of free electrons in samples.

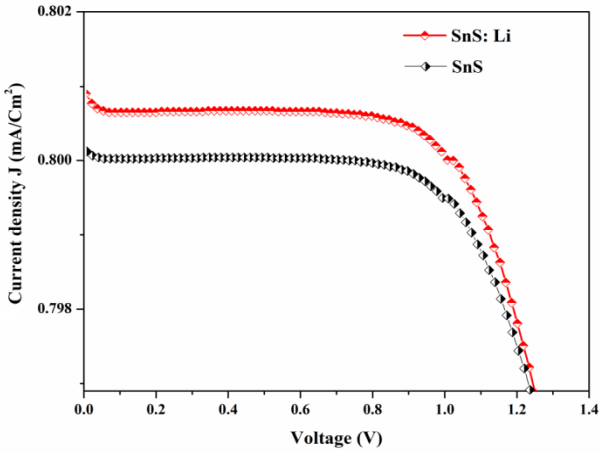

Fig. 11. J-V characteristic curves of the SnS and SnS: Li thin film samples.

The highest surface area nature of SnS and SnS: Li thin films allows for significant electron conduction. A high surface area and good electro catalytic activities are favourable for short-circuit current density (Jsc). As a result, the Jsc displayed is much closer to the conventional value. The fill factor of the SnS thin films was lower than that of the SnS: Li thin films. This is due to the strong series resistance of the created SnS: Li thin films, which is attributable to their thickness and stability. The open-circuit voltage (Voc) of SnS: Li thin films are larger than that of SnS thin films, owing to the created thin films' effective catalytic activity. It is clear from the I-V characteristics that all of the samples have diode characteristics. As a result, Li doped SnS thin films generated using green synthesis approaches exhibit better photodiode properties than other thin film samples, and this property improves as the synthesis technique of the thin film is changed.

Table 4. Photovoltaic parameters of SnS, and SnS: Li thin films.

Sample	V_{oc} (V)	J_{sc} (mA/Cm^2)	$V_{oc}*J_{sc}$	$V_{mp}*$ (V)	J_{mp} (mA/Cm^2)	$V_{max}*J_{max}$	Fill factor	Efficiency η (%)
SnS	1.246	0.801	1.014	0.775	0.8006	0.621	0.6124	6.21
SnS: Li	1.255	0.88	1.0041	0.99	0.801	0.7920	0.7888	7.92

5. Conclusion

Using ultrasonic technique, tin sulphide (SnS) and lithium-incorporated tin sulphide (SnS: Li) nanoparticles have been synthesized. The optical properties of chemical compounds, such as their morphological, and composition properties have been thoroughly investigated. During chemical synthesis, SnS and SnS: Li nanoparticles have improved in their crystallinity and purity. Pure SnS nanoparticles have improved their optical qualities, while Li doped SnS nanoparticles have improved their electrical properties. The incorporation of Li ions into SnS nanoparticles increases their optical and electrical properties, in particular their UV-vis absorbance and their band gap values. These samples can potentially serve as an abundant, sustainable, and ecologically adaptive material for solar energy conversion and storage, based on the obtained results.

References

[1] N.P. Klochko, O.V. Lukianova, V.R. Kopach, I.I. Tyukhov, N.D. Volkova, G.S. Khrypunov, V.M. Lyubov, M.M. Kharchenko, M.V. Kirichenko, Sol. Energy 134, (2016) 156-164; https://doi.org/10.1016/j.solener.2016.04.031

[2] V. Kavitha, P. Mahalingam, M. Jeyanthinath, N. Sethupathi, Mater. Today-Proc. 23 (2020) 12-15; https://doi.org/10.1016/j.matpr.2019.05.351

[3] V. Kavitha, P. Mahalingam, M. Jeyanthinath, N. Sethupathi, Mater Today-Proc. 35 (2021) 48-52; https://doi.org/10.1016/j.matpr.2019.05.437

[4] F. Ballipinar, A.C. Rastogi, J. Alloy. Compd. 728, (2017) 179-188; https://doi.org/10.1016/j.jallcom.2017.08.295

[5] S. Di Mare, D. Menossi, A. Salavei, E. Artegiani, F. Piccinelli, A. Kumar, G. Mariotto, A. Romeo, Coatings 7(2), (2017) 34; https://doi.org/10.3390/coatings7020034

[6] D. Avellaneda, G. Delgado, M.T.S. Nair, P.K. Nair, Thin Solid Films 515(15), (2007) 5771-5776; https://doi.org/10.1016/j.tsf.2006.12.078

[7] M. Parenteau, C. Carlone, Phys. Rev. B 41(8), (1990) 5227-5234; https://doi.org/10.1103/PhysRevB.41.5227

[8] Y. Aimi, K. Takashi, A. Yoji, N. Shigeyuki, O. Hiroto, K. Hironori, A. Hideaki, J. Appl. Phys. 57(2S2), 02CE08 (2018); https://doi.org/10.7567/JJAP.57.02CE08

[9] H. Noguchi, A. Setiyadi, H. Tanamura, T. Nagatomo, O. Omoto, Sol. Energy Mater. Sol. Cells 35, 325-331 (1994); https://doi.org/10.1016/0927-0248(94)90158-9

[10] Y. Zou, Y. Wang, Chem. Eng. J. 229, 183-189 (2013);https://doi.org/10.1016/j.cej.2013.05.119

[11] X. Jiang, X. Yang, Y. Zhu, J. Shen, K. Fan, C. Li, J. Power Sources 237, 178-186 (2013); https://doi.org/10.1016/j.jpowsour.2013.03.048

[12] U. Chalapathi, B. Poornaprakash, Si-Hyun Park, Solar Energy, 139, 2016, 238-248; https://doi.org/10.1016/j.solener.2016.09.046

[13]SreedeviGedi,Vasudeva Reddy, Minnam Reddy, Tulasi Ramakrishna Reddy Kotte,Young sang Park, Woo Kyoung Kim, Applied Surface Science, 465, 2019 802-815; https://doi.org/10.1016/j.apsusc.2018.09.214

[14]S.S.Hegde, A.G.Kunjomana, P.Murahari,B.K.Prasad, K.Ramesh, Surfaces and Interfaces, 10, 2018 78-84; https://doi.org/10.1016/j.surfin.2017.12.003

[15] Krishna RaoEswarNeerugatti, PravinShivajiPawar, JaeyeongHeo, Materials Letters, 284 (2) 2021 129026; https://doi.org/10.1016/j.matlet.2020.129026

[16] A. M. S.Arulanantham, S. Valanarasu, K. Jeyadheepan, V.Ganesh, MohdShkir, Journal of Molecular Structure, 1152 (15) 2018, 137-144; https://doi.org/10.1016/j.molstruc.2017.09.077

[17] Robert W. Miles, Ogah E. Ogah, Guillaume Zoppi, Ian Forbes, Thin Solid Films, 517(17), 2009, 4702-4705; https://doi.org/10.1016/j.tsf.2009.03.003

[18] S. Weidong, H. Lihua, W. Haishui, Z. Hongjie, Y. Jianhui, W. Pinghui, Nanotechnology 17(12), (2006) 2918; https://doi.org/10.1088/0957-4484/17/12/016

[19] W. Anaf, O. Schalm, K. Janssens, K. De Wael, Dyes Pigm. 113, (2015) 409-415; https://doi.org/10.1016/j.dyepig.2014.09.015

[20] K. Hartman, J.L. Johnson, M.I. Bertoni, D. Recht, M.J. Aziz, M.A. Scarpulla, T. Buonassisi, Thin Solid Films 519(21), (2011)7421-7424; https://doi.org/10.1016/j.tsf.2010.12.186

[21] M. Devika, N.K. Reddy, K. Ramesh, V. Ganesan, E. Gopal, K.R. Reddy, Appl. Surf. Sci. 253(3), (2006) 1673-1676; https://doi.org/10.1016/j.apsusc.2006.03.005

[22] A. Tanuševski, D. Poelman, Solar Energy Mater. Solar Cells 80(3), (2003) 297-303; https://doi.org/10.1016/j.solmat.2003.06.002

[23] C. Gao, H. Shen, L. Sun, H. Huang, L. Lu, H. Cai, Mater. Lett. 64(20), 2177-2179 (2010); https://doi.org/10.1016/j.matlet.2010.07.002

[24] C. Gao, H. Shen, Thin Solid Films 520(9), (2012) 3523-3527;

https://doi.org/10.1016/j.tsf.2011.12.077
[25] V. Dhanasekaran, T. Mahalingam, J.K. Rhee, J. Chu, J. Adv. Microsc. Res. 6(2), 126-130 (2011); https://doi.org/10.1166/jamr.2011.1065
[26] K. C. Suresh, S. Surendhiran, P. Manoj Kumar, E. Ranjth Kumar, Y. A. Syed Khadar, A. Balamurugan, SN Appl. Sci. 2 (2020) 1-13; https://doi.org/10.1007/s42452-020-03534-z
[27] K. Kandasamy, S. Surendhiran, Y.A. Syed Khadar, P. Rajasingh, Mater. Today-Proc. 47 (2020) 757-762; https://doi.org/10.1016/j.matpr.2020.07.080
[28] A. Balamurugan, M. Sudha, S. Surendhiran, R. Anandarasu, S. Ravikumar, Y.A. Syed Khadar, Mater. Today-Proc. 26:4 (2020) 3588-3594; https://doi.org/10.1016/j.matpr.2019.08.217
[29] K.D.A. Kumar, S. Valanarasu, K. Jeyadheepan, H.-S. Kim, D. Vikraman, J. Mater. Sci.: Mater. Electron. 29(5), (2018) 3648-3656; https://doi.org/10.1007/s10854-017-8295-2
[30] V. Gremenok, V.Y. Rud, Y.V. Rud, S. Bashkirov, V. Ivanov, Semiconductors 45(8), (2011) 1053; https://doi.org/10.1134/S1063782611080094
[31] Y.A. Syed Khadar, A. Balamurugan, V.P. Devarajan R. Subramanian, S. Dinesh Kumar, J. Mater. Res. Technol. 8:1 (2019) 267-274; https://doi.org/10.1016/j.jmrt.2017.12.005
[32] K. C. Suresh, A. Balamurugan, Inorg. Nano-Met. Chem. 51:2 (2021) 1-6; https://doi.org/10.1080/24701556.2020.1770793
[33] M. Indhumathy, A. Prakasam, Journal of Materials Science: Materials in Electronics, 30, (2019) 15444-15451; https://doi.org/10.1007/s10854-019-01920-x
[34] S. Zhang, S.Y. Cheng, H.J. Jia, H.F. Zhou, Adv. Mater. Res. 418-420, (2012); 712-716; https://doi.org/10.4028/www.scientific.net/AMR.418-420.712
[35] M. Devika, N.K. Reddy, K. Ramesh, K. Gunasekhar, E. Gopal, K.R. Reddy, J. Electrochem. Soc. 153(8), (2006) G727-G733; https://doi.org/10.1149/1.2204870
[36]NannanMeng, Yifeng Zhou, WangyanNie, Pengpeng Chen, J Nanopart Res (2016) 18:241
[37]Jiahong Wang, Shan Liang, Liang Ma, Sijing Ding, Xuefeng Yu, Li Zhoua and Ququan Wang, CrystEngComm, 2014, 16, 399; https://doi.org/10.1039/C3CE41807C
[38] Arvind Singh, A.S.K. Sinha, Applied Surface Science 430 (2018) 184-197; https://doi.org/10.1016/j.apsusc.2017.02.214
[39] S. Palanisamy, N. Rajendhran, S. Srinivasan, A.P. Shyma, V. Murugan, B. Parasuraman, S. Kheawhom, J. Appl. Electrochem. 51 (2021) 345-356; https://doi.org/10.1007/s10800-020-01493-2
[40] S. Palanisamy, S. Srinivasan, SN Appl. Sci. 1 (2019) 837;https://doi.org/10.1007/s42452-019-0846-0
[41] M. Sudha, S. Surendhiran, V. Gowthambabu, A. Balamurugan, R. Anandarasu, Y. A. Syed Khadar, D. Vasudevan, J. Bio. Tribocorros. 7:60 (2021) 1-16; https://doi.org/10.1007/s40735-021-00492-w
[42] D. Vasudevan, D. Senthilkumar, S. Surendhiran, Int. J. Thermophys. 41:74 (2020) 1-19; https://doi.org/10.1007/s10765-020-02651-6
[43] K. Santhosh Kumar, C. Manoharan, S. Dhanapandian, A. GowriManohari, Spectrochim. Acta Part A 115, (2013) 840-844; https://doi.org/10.1016/j.saa.2013.06.112
[44] M. Reghima, A. Akkari, C. Guasch, N. Kamoun-Turki, J. Renew. Sustain. Energy 4(1), (2012) 011602; https://doi.org/10.1063/1.3676073
[45] Yi Niu, Yide Chen, Jing Jiang, Yan Pan, Chengcheng Yang, Chao Wang, IOP Conf. Series: Materials Science and Engineering 738 (2020) 012016; https://doi.org/10.1088/1757-899X/738/1/012016